Direct Time-Domain View of Auger Recombination in a Semiconductor

Kristopher W. Williams, Nicholas R. Monahan, Tyler J. S. Evans, and X.-Y. Zhu*
Department of Chemistry, Columbia University, New York, New York 10027, USA
(Received 6 October 2016; published 24 February 2017)

The radiationless recombination of electron-hole pairs in semiconductors is detrimental to optoelectronic technologies. A prominent mechanism is Auger recombination, in which nonradiative recombination occurs efficiently by transferring the released energy-momentum to a third charge carrier. Here we use femtosecond photoemission to directly detect Auger electrons as they scatter into energy and momentum spaces from Auger recombination in a model semiconductor, GaSb. The Auger rate is modulated by a coherent phonon mode at 2 THz, confirming phonon participation in momentum conservation. The commonly assumed Auger rate constant is found not to be a constant, but rather decreases by 4 orders of magnitude as hot electrons cool down by ~90 meV. These findings provide quantitative guidance in understanding Auger recombination and in designing materials for efficient optoelectronics.

DOI: 10.1103/PhysRevLett.118.087402

Light-emitting diodes (LEDs) and semiconductor lasers function by converting injected charges into photons. Their efficiencies are limited at high charge densities by nonradiative loss channels, as exemplified by the well-known efficiency "droop" problem in LEDs [1,2]. Prominent among the loss mechanisms are the device specific electron-leakage and the intrinsic Auger recombination [1,2]. The later [3–7], proposed since the 1950s [8,9], is believed to be either direct Auger recombination (DAR) [8–10], in which an electron and a hole nonradiatively recombine and transfer the released energy to a third electron or hole, or phonon-assisted Auger recombination (PAAR) [11–17], in which energy-momentum conservation occurs with the absorption or emission of a phonon. Despite decades of research, the Auger recombination mechanism remains poorly understood. This can be attributed in a major part to the indirect nature of most experimental evidence, such as the third-order dependence of the photoluminescence (PL) decay rate on carrier density [1–3], with only a few attempts at more direct observations with limited time and/or energy resolutions [14,18–22]. Here we use femtosecond time-resolved two-photon photoemission (TR-2PPE) to directly detect Auger electrons as they scatter into energy and momentum spaces expected from Auger recombination in p-GaSb. The Auger rate is modulated by a coherent phonon mode at 2 THz, confirming phonon participation in momentum conservation. The commonly assumed Auger rate constant is found not to be a constant, but rather decreases by $\times 10^4$ as hot electrons cool down by ~90 meV. Moreover, we show the third-order Auger process can appear as a rate-limiting first-order process in excitation density due to intervalley scattering.

We choose GaSb as the model system because the Auger rate is high due to the small band gap [23], the predicted importance of the PAAR mechanism [17], and the large difference in the effective masses ($m_{\mathrm{HH}}/m_{\mathrm{CB}} \approx 10$) between the heavy-hole (HH) valence band (VB) and the conduction band (CB) [24,25]. The latter condition aids in momentum conservation by providing a large number of momentum states available for scattering without significant change to energy conservation [26]. The favorable conditions for Auger recombination in GaSb allow us to directly detect Auger electrons in TR-2PPE from e-e-h Auger scattering events. For comparison, our previous TR-2PPE measurement on the technologically important InGaN quantum well system failed to detect Auger electrons [4] due to the much lower Auger rate in InGaN than that in GaSb.

Experimental details can be found in the Supplemental Material [27]. Briefly, the samples were cut from polished GaSb wafers (MTI Corporation) with (100) orientation and p-type doping (Zn, $2.0–5.0 \times 10^{18}$ cm^{-3}). The clean GaSb(100) surfaces were obtained from sputter-anneal cycles to produce (1×3) reconstructed surfaces (Fig. S1). The band gap of $E_g = 0.71$ eV at room temperature was determined from optical absorption (Fig. S2). In the TR-2PPE experiments presented below, a portion of a Yb-doped fiber laser (Clark-MXR IMPULSE) was used as the near-IR pump pulse ($h\nu_1 = 1.19$ eV, 32 ± 5 fs, 2.0–21.3 W/cm^2) while the remainder was used to generate the UV probe ($h\nu_2 = 4.51$ eV, 91 ± 2 fs, 0.2 W/cm^2) from a homebuilt noncollinear optical parametric amplifier (NOPA). We measure the kinetic energy and parallel momentum of the photoemitted electrons using a hemispherical electron energy analyzer (VG Scienta, R3000). This analyzer was also used, in conjunction with a He-I UV source ($h\nu_1 = 21.2$ eV), for angle-resolved photoemission spectroscopy (ARPES, Fig. S3), which confirmed the dispersion of the valence subbands and a valence band maximum (VBM) 0.08 eV below the Fermi level (E_F). This puts the absolute conduction band minimum (CBM) energy at 0.63 eV above E_F. A sample temperature of 114 K was used in TR-2PPE measurements.

Auger recombination.—Following the above band gap excitation by $h\nu_1$, electrons accumulate near the CBM and holes near VBM (Γ point for GaSb). An *e-e-h* Auger scattering process, DAR [Fig. 1(a)] or PAAR [Fig. 1(b)], results in an Auger electron with excess energy of at least E_g (0.71 eV) above the CBM.

Figure 1(c) shows a pseudocolor plot of the TR-2PPE spectra ($h\nu_1 = 1.19$ and $h\nu_2 = 4.51$ eV) as a function of pump-probe delay (Δt). We observe (i) the rise on the ps time scale of the electron population at or near the CBM that remains nearly constant at longer times and (ii) concurrent with the rise in the CBM signal, the growth of a high energy electron distribution extending to ~1 eV above the CBM at short time delays. This is clear in horizontal cuts from the CBM distribution at 0.79 ± 0.1 eV and the high energy electrons at 1.36 ± 0.05 eV, Fig. 1(d). The CBM signal grows on the ps time scale and reaches a nearly steady-state value (slow increase) for $\Delta t \geq 5$ ps. Photoemission intensity of the high energy electrons also grows over 2 ps after excitation and then rapidly decreases to a nearly steady state signal 1 order of magnitude lower than the peak. Given the pump pulse duration of 0.3 ps, we can eliminate the possibility of two-photon absorption as the source of high-energy electrons. The slow generation of high-energy electrons, along with the observation of proper energy and momentum conservation (below), confirms the direct detection of the Auger recombination mechanism. The decrease in Auger electron intensity for $\Delta t > 2$ ps results from the strong dependence of Auger rates on electron energy, as detailed later in Fig. 3.

Figure 1(e) compares 2PPE spectra (logarithmic scale) at pump-probe delays $\Delta t = 0.6$, 2.0, 3.5, and 6.0 ps. The high-energy Auger electron feature grows initially (0.6 ps) with CBM population, peaks at 2 ps, and decays at longer times. The Auger electron feature is not a distinct peak, but rather a broad distribution extending to ~1 eV above CBM. The excess energy is expected from the energy conserved scattering of hot electrons from an *e-e-h* Auger mechanism. The broad distribution is also expected as electrons with such high excess energy cool down on the femtosecond time scale via scattering with LO phonons [30]. Within the limited time resolution, we are detecting not just nascent Auger electrons, but mostly electrons that have cooled due to inelastic scattering with LO phonons.

Further evidence comes from angle-resolved measurement. Momentum conservation necessarily results in Auger electrons in states with a higher momentum than those near the band edge [Figs. 1(a) and 1(b)]. Figure 1(f) shows the parallel-momentum dependence of the CB and Auger photoemission signals, where $k_{\|} = 0$ Å^{-1} is the Γ point. The signal from electrons near the CBM decreases quickly with increasing $k_{\|}$, as expected for the highly dispersive CB in GaSb. The signal from Auger electrons, however, extends much further into k space due to the occupation of high momentum states. Significant Auger electron

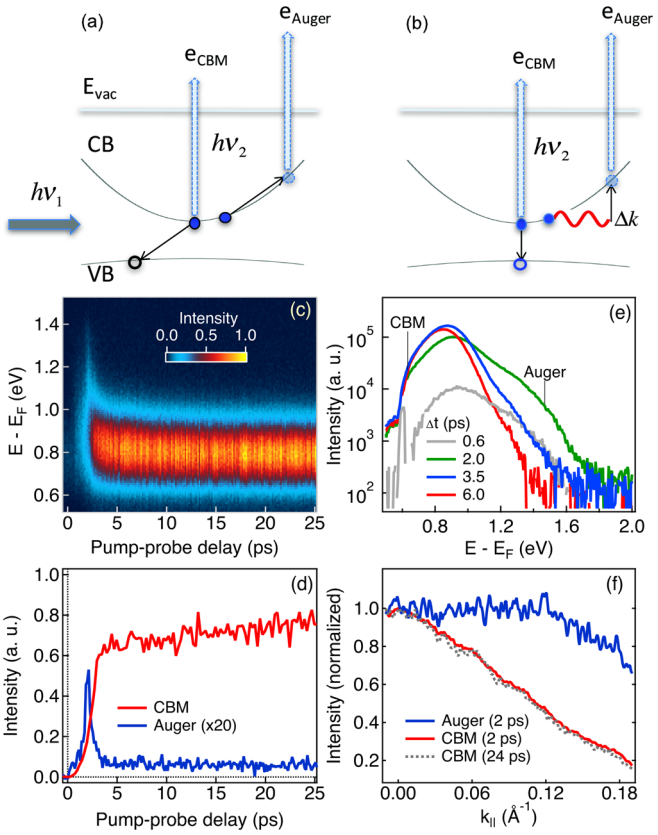

FIG. 1. Direct detection of *e-e-h* Auger recombination by 2PPE. Top: Detection of Auger recombination from the (a) DAR or (b) PAAR mechanism by TR-2PPE. Following excitation by the pump ($h\nu_1$) to initiate the Auger process, the probe ($h\nu_2$) ionizes the Auger or CBM electron. The difference between DAR and PAAR is the participation of a phonon (red wavy line) for momentum conservation (Δk) in the latter. (c) Pseudocolor (intensity) plot of TR-2PPE spectra ($h\nu_1 = 1.19$ and $h\nu_2 = 4.51$ eV) at an excitation density of 1.3×10^{18} cm^{-3}; (d) kinetic profiles from horizontal cuts of the 2D plot at 0.79 ± 0.1 (CBM) and 1.36 ± 0.05 eV (Auger); (e) TR-2PPE spectra at selected pump-probe delays ($\Delta t = 0.6$–6 ps); (f) parallel momentum-resolved TR-2PPE for the Auger (blue) and CBM (red) electrons at $\Delta t = 2$ ps. Also shown is data for CBM at $\Delta t = 24$ ps (gray dots).

intensity is seen even at $k_{\|} = 0$ Å^{-1}. This is attributed to the projection of high momentum states in the bulk Brillouin zone onto the surface Brillouin zone (SBZ) detected in photoemission experiments [31]. Heavy *X*-valley states, initially populated due to intervalley scattering from the above-gap photoexcitation, may also contribute to the photoemission signal due to projection onto the SBZ; however, the *X*-valley minimum would only contribute signal at a much lower energy (~300 meV above CBM) than those of the Auger electron measured here and is depopulated due to subpicosecond intervalley scattering to the lower lying *L* valley [32,33].

Phonon participation.—A close examination of the kinetic profiles in Fig. 1(d) shows the appearance of oscillations in the rising Auger electron signal, Fig. 2(a).

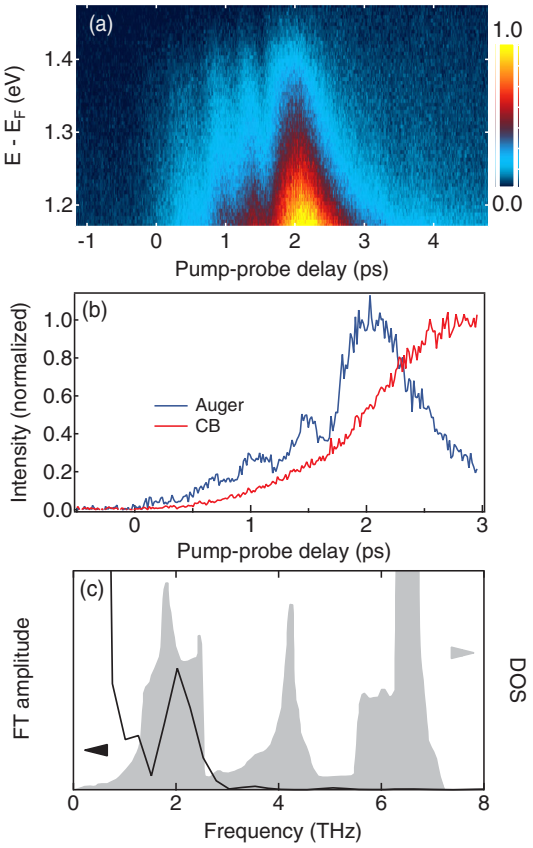

FIG. 2. Direct evidence for PAAR. (a) A high resolution expanded view of TR-2PPE spectra ($h\nu_1 = 1.19$, $h\nu_2 = 4.51$ eV; excitation density $= 1.5 \times 10^{18}$ cm^{-3}) in the high energy Auger electron window at short times showing the oscillatory behavior; (b) a comparison of kinetic profiles of Auger electron intensity (blue) and CBM electron intensity (red), with oscillatory behavior only for the former; (c) Fourier transform (black curve) of the kinetic profile of Auger electrons and the calculated density-of-states (DOS, right axis) distribution of phonons in GaSb from Ref. [34].

The time-dependent intensity of the high-energy Auger electrons is periodically modulated with a time constant of 0.50 ± 0.08 ps. A comparison of the kinetic profiles of the Auger electrons (1.36 ± 0.05 eV, blue) and those near the CBM (0.79 ± 0.1 eV, red), Fig. 2(b), shows the oscillatory component only in the former. The regular period of the oscillation indicates the involvement of a coherent phonon, which is launched by the short pump pulse. Since the rise of the Auger electron signal follows that of CB over ~2 ps, we subtract the two normalized kinetic profiles to better isolate the oscillatory component and then Fourier transform the difference. The Fourier transform [black curve in Fig. 2(c)] clearly reveals that the oscillation in Auger signal is dominated by a frequency at 2.0 ± 0.3 THz, which lies within the lowest energy peak in the calculated phonon density of states (DOS) for GaSb [34]. This 2 THz component corresponding to the dominant acoustic phonon band.

The oscillation in the rise of the Auger electron signal reveals the modulation of the Auger scattering rate by participation of the coherent phonon in the PAAR mechanism. Here, the time-dependent electron-phonon interaction—observable due to the coherence of the oscillating displacement field—acts to modulate the momentum vector [Δk in Fig. 1(b)] available to carriers and thus the Auger rate [35,36]. Note that other higher frequency phonon modes may also be involved, albeit not resolved due to limited time resolution.

Strong dependence on carrier energy.—To obtain the relative Auger rate constant, k_{Aug}, we take the 2PPE intensity near the CBM as directly proportional to CB electron density [n_e] and that of the high-energy electrons to the transient density of Auger electrons [n_{Aug}]. Because the rate of decay for Auger electrons out of the energy window of detection, due to scattering with LO phonons on the femtosecond time scale [30], is much higher than the rate of formation (~ps), we use the steady state approximation for [n_{Aug}] to show (see Supplemental Material, Sec. S3 [27]):

$$[n_{\mathrm{Aug}}] = \frac{k_{\mathrm{Aug}}}{k_d}[n_e]^2[n_h] \propto k_{\mathrm{Aug}}[n_e]^2, \tag{1}$$

where the VB hole density [n_h] is taken to be constant within the experimental time window as there are no interband scattering channels and radiative recombination occurs on ns time scales. [n_e] is the time-dependent CB electron density resulting from intervalley scattering as described below, and k_d is the first order rate constant for the decay of Auger electrons out of the energy window of detection. From Eq. (1), we obtain the relative k_{Aug} by taking the ratio of the 2PPE intensity for the high energy Auger electrons and the square of that near the CBM. The result is shown in Fig. 3(a) (red and orange crosses, left axis, logarithmic scale) for k_{Aug} (normalized to average value at 10–20 ps) as a function of Δt. The k_{Aug} value decreases with increasing time by 3-4 orders of magnitude and reaches a nearly constant value for $\Delta t \geq 5$ ps. The excellent correlation between the Auger rate constant on a logarithmic scale and the hot electron energy on a linear scale above a certain threshold suggests an exponential function of the former on the latter. Here we represent the mean electron energy by the quasi-Fermi level, E^*_{Fermi} (blue, open circles, right axis). We obtain E^*_{Fermi} by deconvolving the main electron distribution near the CBM from that of the Auger electrons, as detailed in the Supplemental Material (Fig. S5) [27]. We find that k_{Aug} closely tracks E^*_{Fermi} within the first 5 ps and divergence is only obvious for $\Delta t \geq 5$ ps. Figure 3(b) plots k_{Aug} (black circles) vs the mean energy of electrons near the CBM, $\langle E_{\mathrm{CB}} \rangle$, as obtained from the TR-2PPE spectra with deconvolution to remove the small contribution of the high energy Auger electrons. As $\langle E_{\mathrm{CB}} \rangle$ increases by ~90 meV from ~0.15 eV

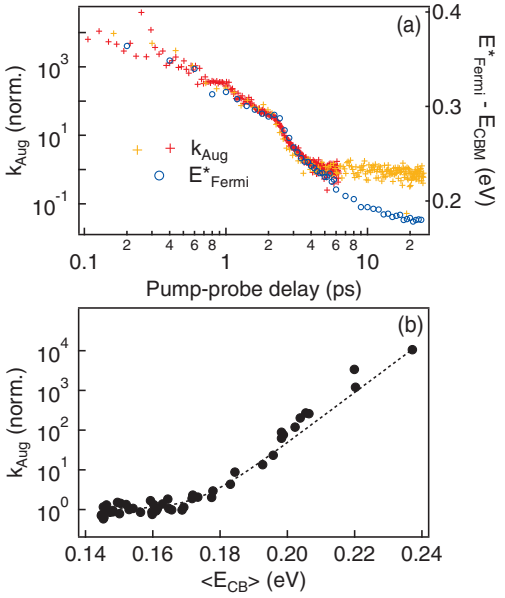

FIG. 3. Energy dependent Auger rates. Upper: Auger recombination rate constant (crosses, normalized to the average values at $\Delta t = 10$–20 ps) as a function of Δt. The two sets of data are obtained with high (red) and low (orange) time resolutions. Also shown is the change in the quasi-Fermi level (E^*_{Fermi}, right axis) of the electron distribution near CBM as a function of Δt. Lower: relative Auger rate as a function of the average energy of CBM electrons (dots, referenced to CBM). The dashed curve is an exponential fit with X offset of 0.145 ± 0.005 eV.

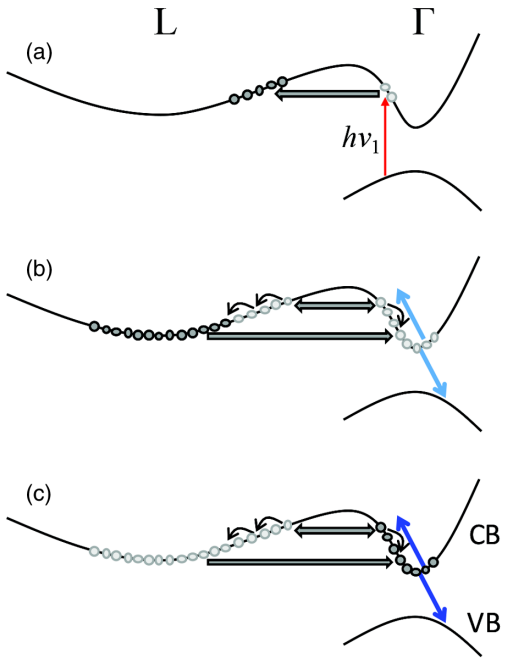

FIG. 4. Intervalley scattering and rate-limited Auger recombination. (a)–(c) Increasing time after initial photoexcitation.

to 0.24 eV, k_{Aug} increases by ~4 orders of magnitude and the data can be well approximated by an exponential function (dashed curve) as suggested above. Note that the CB electron distribution remains nonthermal at 25 ps and this has been attributed to Auger heating [18].

The results in Fig. 3 illustrate the extreme sensitivity of the Auger scattering process to energy-momentum conservation. While an increase in the Auger constant across 2 orders of magnitude with sample temperature has been reported in Si nanowires and attributed to phonons [37], our results on GaSb show that the increase in k_{Aug} arises from an increase in carrier temperature. This effect is particularly important for the DAR mechanism, in which a hotter carrier distribution provides a broader phase space for Auger scattering that simultaneously satisfies energy and momentum conservation. This finding suggests that Auger recombination can be dominated by nonequilibrium hot carriers from charge injection or by the broad tails of the (electronically) thermalized carrier distributions at high carrier densities in LEDs or lasers. This finding may also explain why the transient Auger rate constants measured in time-resolved photoemission on femto- to picosecond time scales are many orders of magnitude higher than the phenomenological rate constants from luminescence quantum yield measurements [4,38]. We point out that most experimental [3,5,37,38] and theoretical or computational studies [6,7,14,15,17] have assumed k_{Aug} as a constant.

Rate-limiting Auger recombination.—The initial rise in electron population near the CBM and the concurrent rise in Auger electron population can be attributed to the unique band structure of GaSb. As shown in Fig. 4(a), photoexcitation creates electrons in the Γ valley, with excess energy above the intervalley threshold (63–100 meV) [39], that are quickly scattered to L due to the large effective mass ($m_{Ll} = 1.3\, m_e$ and $m_{Lt} = 0.10\, m_e$), and thus high DOS, in the L valley [39–41], leaving <5% of excited electrons in the Γ valley in $\leq 10^2$ fs so that carrier cooling occurs predominately within the L valley [18,29]. In contrast, holes stay near the VBM in the Γ valley. Scattering of electrons back to Γ is slower due to the lower DOS ($m_\Gamma = 0.039 m_e$) and state blocking [39,40]. Since photoemission probes a limited crystal momentum space near Γ, the intervalley scattering process is responsible for the observed rise in CBM intensity [Fig. 2(b)]. The Auger recombination process is initiated as the CB electrons accumulate near the CBM [Fig. 4(b)] and peaks at 2 ps when there is sufficiently high CBM electron population combined with excess electron energy [Fig. 4(c)]. Auger recombination, a third-order process in carrier density, therefore depends on the first-order intervalley backscattering of electrons from L to Γ. The Auger mechanism is rate limited to an apparent first-order process in excitation density (see Supplemental Material, Sec. S4), as confirmed in power dependence (Fig. S4) [27]. Such a rate-limiting Auger recombination process suggests a mechanism to increase the efficiency of LEDs at high injection densities (Supplemental Material, Sec. S7) through band structure engineering [42].

Summary.—The results presented above show the direct detection of Auger electrons and the confirmation of phonon participation as a momentum conservation mechanism. We reveal the critical dependence of the Auger rate constant on hot carrier energy: the Auger recombination rate constant increases by as much as 10^4 as the hot carrier energy increases by ~90 meV in the conduction band. Thus, the prevailing models of using phenomenological Auger recombination rate constants that are time and energy independent are of limited validity.

X. Y. Z. acknowledges support by the U.S. Department of Energy Grant No. DE-SC0014563 for the TR-2PPE experiments. Partial support for sample preparation and characterization by the Samsung Global Research Opportunity program is also acknowledged. We thank D. Reichman and I. Dunn for fruitful discussions.

*To whom correspondence should be addressed.
xyzhu@columbia.edu

[1] J. Piprek, Phys. Status Solidi A **207**, 2217 (2010).
[2] G. Verzellesi, D. Saguatti, M. Meneghini, F. Bertazzi, M. Goano, G. Meneghesso, and E. Zanoni, J. Appl. Phys. **114**, 071101 (2013).
[3] Y. C. Shen, G. O. Mueller, S. Watanabe, N. F. Gardner, A. Munkholm, and M. R. Krames, Appl. Phys. Lett. **91**, 141101 (2007).
[4] K. W. Williams, N. R. Monahan, D. D. Koleske, M. H. Crawford, and X.-Y. Zhu, Appl. Phys. Lett. **108**, 141105 (2016).
[5] M. Binder, A. Nirschl, R. Zeisel, T. Hager, H. J. Lugauer, M. Sabathil, D. Bougeard, J. Wagner, and B. Galler, Appl. Phys. Lett. **103**, 071108 (2013).
[6] E. Kioupakis, P. Rinke, K. T. Delaney, and C. G. Van De Walle, Appl. Phys. Lett. **98**, 161107 (2016).
[7] R. Vaxenburg, A. Rodina, E. Lifshitz, and A. L. Efros, Appl. Phys. Lett. **103**, 221111 (2013).
[8] H. Fröhlich and J. O'Dwyer, Proc. Phys. Soc. London Sect. A **63**, 81 (1950).
[9] A. R. Beattie and P. T. Landsberg, Proc. R. Soc. A **249**, 16 (1959).
[10] Y. C. Shen, G. O. Mueller, S. Watanabe, N. F. Gardner, a. Munkholm, and M. R. Krames, Appl. Phys. Lett. **91**, 141101 (2007).
[11] R. Conradt and W. Waidelich, Phys. Rev. Lett. **20**, 8 (1968).
[12] L. Huldt, Phys. Status Solidi A **8**, 173 (1971).
[13] L. Huldt, Phys. Status Solidi A **24**, 221 (1974).
[14] G. Benz and R. Conradt, Phys. Rev. B **16**, 843 (1977).
[15] W. Lochmann, Phys. Status Solidi A **40**, 285 (1977).
[16] M. Takeshima, Phys. Rev. B **25**, 5390 (1982).
[17] M. Takeshima, Phys. Rev. B **23**, 6625 (1981).
[18] P. A. Snow, D. J. Westland, J. F. Ryan, T. Kerr, H. Munekata, and L. L. Chang, Superlattices Microstruct. **5**, 595 (1989).
[19] J. I. Pankove, L. Tomasetta, and B. F. Williams, Phys. Rev. Lett. **27**, 29 (1971).
[20] J. Iveland, L. Martinelli, J. Peretti, J. S. Speck, and C. Weisbuch, Phys. Rev. Lett. **110**, 177406 (2013).
[21] J. Iveland, M. Piccardo, L. Martinelli, J. Peretti, J. W. Choi, N. Young, S. Nakamura, J. S. Speck, and C. Weisbuch, Appl. Phys. Lett. **105**, 052103 (2014).
[22] F. Bertazzi, M. Goano, X. Zhou, M. Calciati, G. Ghione, M. Matsubara, and E. Bellotti, Appl. Phys. Lett. **106**, 061112 (2015).
[23] C. Ghezzi, R. Magnanini, A. Parisini, B. Rotelli, L. Tarricone, A. Bosacchi, and S. Franchi, Phys. Rev. B **52**, 1463 (1995).
[24] M. Reine, R. L. Aggarwal, and B. Lax, Phys. Rev. B **5**, 3033 (1972).
[25] A. Filion and E. Fortin, Phys. Rev. B **8**, 3852 (1973).
[26] J. T. Olesberg and M. E. Flatté, *Mid-infrared Semiconductor Optoelectronics* (Springer, London, 2006), p. 3.
[27] See Supplemental Material at http://link.aps.org/supplemental/10.1103/PhysRevLett.118.087402 for sample details, preparation, and characterization, kinetic analysis, deconvolution model, and experimental details, which includes Refs. [18,28,29].
[28] C. Xu and W. W. Webb, J. Opt. Soc. Am. B **13**, 481 (1996).
[29] P. A. Snow, P. Maly, D. J. Westland, and J. R. Ryan, Solid State Electron. **32**, 1485 (1989).
[30] J. Shah and R. F. Leheny, *Semiconductors Probed by Ultrafast Laser Spectroscopy* (Academic Press, Inc, Orlando, 1984), p. 45.
[31] S. Hüfner, *Photoelectron Spectroscopy* (Springer, Berlin, Heidelberg, 2003).
[32] S. Zollner, S. Gopalan, and M. Cardona, Appl. Phys. Lett. **54**, 614 (1989).
[33] S. Zollner, S. Gopalan, and M. Cardona, J. Appl. Phys. **68**, 1682 (1990).
[34] P. Giannozzi, S. de Gironcoli, P. Pavone, and S. Baroni, Phys. Rev. B **43**, 7231 (1991).
[35] W. Lochmann, Phys. Status Solidi **42**, 181 (1977).
[36] U. Rössler, *Solid State Theory: An Introduction* (Springer, Berlin, Heidelberg, 2004), p. 223.
[37] A. R. Guichard, R. D. Kekatpure, M. L. Brongersma, and T. I. Kamins, Phys. Rev. B **78**, 235422 (2008).
[38] H. Tanimura, J. Kanasaki, and K. Tanimura, Phys. Rev. B **91**, 045201 (2015).
[39] I. Vurgaftman, J. R. Meyer, and L. R. Ram-Mohan, J. Appl. Phys. **89**, 5815 (2001).
[40] W. S. Pelouch and L. A. Schlie, Appl. Phys. Lett. **66**, 82 (1995).
[41] D. C. Smith, E. D. O'Sullivan, L. Rota, A. C. Maciel, and J. F. Ryan, Phys. Status Solidi B **204**, 110 (1997).
[42] K. J. Cheetham, A. Krier, I. P. Marko, A. Aldukhayel, and S. J. Sweeney, Appl. Phys. Lett. **99**, 141110 (2011).